Coupling Between Highly Conducting and Permeable Metallic Objects in the EMI Frequency Range

F. Shubitidze [1], K. O'Neill [1,2], I. Shamatava [1], and K. Sun [1]
[1] Thayer School of Engineering, Dartmouth College,
Cummings Hall, HB 8000, Hanover NH, 03755, USA
e-mail: fridon.shubitidze@dartmouth.edu
Tel: 603 646 3671; Fax: 603 646 3856

[2] USA ERDC Cold Regions Research and Engineering Laboratory,
72 Lyme Road, Hanover NH, 03755, USA

Abstract - Electromagnetic induction (EMI) sensing, from 10's of Hz up to 100's of kHz, is emerging as one of the most promising remote sensing technologies for detection and discrimination of buried metallic objects, particularly unexploded ordinance (UXO). For a single homogenous target it has been shown that the scattered EMI signal strongly depends on an object's geometry and its electromagnetic parameters. Most if not all UXO contain different kinds of metal. Additionally, UXO sites are often highly contaminated with metallic clutter. Methods are currently needed to distinguish dangerous objects, such as UXO, from innocuous clutter. Recently, analysis of broadband EMI responses from multiple objects has demonstrated significant interaction between them. The main goal of the paper is to investigate interaction phenomena between highly conducting and permeable metallic objects in the EMI frequency range. Numerical results are compared with experimental data for canonical geometries (spheres and cylinders). The results indicate when and how interaction affects the EMI responses and provides guidance for use of this understanding for future target discrimination purposes.

Keywords: UXO, Low frequency, Electromagnetic induction, Auxiliary sources, Interaction, multiple, scattering.

I. Introduction

Cleaning up buried unexploded ordinance has been identified as a very high priority environmental problem for many years. A significant fraction of all ordinance fired does not detonate and remains dangerous for a long time. In some cases, the ordinance is broken in parts upon impact with the ground, complicating discrimination and possibly contaminating ground water with explosive residues. Most if not all UXO are composite objects with distinct, relatively homogeneous sections, each consisting of different metal shown in Fig. 1, e.g., head, body, tail and fins, copper banding, etc. Further, in many highly contaminated sites, multiple UXO together with widespread clutter appear simultaneously within the field of view of the sensor. The false alarm rate produced by clutter is extremely high and typically causes the majority of remediation costs to be spent on excavating innocuous items. At present the major problem is discrimination not detection. One of most promising technologies for UXO discrimination is electromagnetic induction (EMI) sensing, operating from 10's of Hz up to 100's of kHz. EMI sensing has some distinct advantages relative to ground penetrating radar (GPR): while still range limited, practical depth of penetration of EMI signals is typically not limited by the lossiness of conductive soils, and signal clutter due to dielectric heterogeneity is negligible. At the same time, approaches to processing and resolution improvement that are well established for GPR do not carry over to EMI surveying. Frequency domain EMI responses typically are characterized using two components: one inphase with the primary magnetic field and the other quadrature part and they depend on an object's geometry and it's EM parameters [1], [2].

The magnetic fields radiated by both the sensor and the object fall off very sharply as a function of distance, $\sim 1/R^3$. Therefore, the sensor affects different materials and sections of the target differently. The transmitted ("primary") field produces much stronger excitation of the closest portion of the target. In turn, the parts of the target radiating closest to the receiver disproportionately influence on the scattered signal. These proximity effects are particularly important for identification and discrimination of multiple and composite objects. Analytical techniques based on simple resonating magnetic and electric dipoles are insufficient [3], when sensors pass close to the target, as is often the case in UXO surveying.

Fig. 1. 120 mm HEAT round UXO consists of four sections, altogether about 80 cm long: 1) magnetic (steel), 2) non-magnetic titanium, 3) steel, and 4) aluminum.

The physics of UWB (1Hz – 300kHz) EMI phenomena is of diffusion rather than wave propagation. In general, in the EMI realm displacement currents can be neglected in both target

and surrounding media (air, ground). This means that the dielectric constant of the surrounding medium is typically unimportant for EMI identification of buried targets such as UXO and competing clutter. Soil conductivity is nine orders of magnitude lower than conductivity of a scatterer, which combine with weak electric fields produce only weak soil currents. This means that the exterior (soil) magnetic fields are irrotational, and can thus be represented efficiently using a simple scalar potential. Here we proceed in terms of such potential outside the target, while retaining a vector field formulation inside the metallic object, which an external transmitted ("primary" or excitation) magnetic field may penetrate significantly.

The main goal of the paper is to investigate interaction between highly conducting and permeable metallic sizable objects in the EMI frequency range; and further, to provide the understanding of why, when, and how the interaction affects the EMI response; and finally, to interpret data meaningfully for target classification purposes.

II. A Hybrid Full MAS and MAS-TSA Method for Multiple Targets

Assume that highly conducting and permeable multiple metallic objects $\ell = 1,2,...,N_{ob}$ (where N_{ob} is the number of objects) are placed in a uniform background with the electromagnetic properties effectively of free space. The objects are illuminated by a time varying primary magnetic field and are characterized by relative permeabilities $\mu_{\ell,r}$ and conductivities σ_ℓ [S/m]. The time dependence expression of $e^{j\omega t}$ is suppressed subsequently. The region external to the objects is region 0, and region internal to the ℓ object is region ℓ. Let $\hat{\mathbf{n}}_\ell$ to be outward pointing, normal unit vector to the boundary S_ℓ lying between region 0 and ℓ-th region as shown in Fig. 2. The primary magnetic field penetrates inside objects to some degree, inducing currents within and producing secondary/scattered fields outside. It is very well established that, in the magneto-quasistatic regime, displacement currents $j\omega\mathbf{D}$ can be neglected in comparison with conduction currents within objects. Outside of the targets, the electric field is small. This means that Ampere's Law becomes a homogeneous equation, $\nabla\times\mathbf{H}=0$. The magnetic field in region 0 is irrotational and can be represented as the gradient of a scalar potential. The magnetic field in region ℓ satisfies vector wave equation:

$$\nabla\times\nabla\times\mathbf{H}_\ell - k_\ell^2\mathbf{H}_\ell = 0, \qquad (1)$$

where $k_\ell = \sqrt{-j2\pi\nu\mu_o\mu_{\ell,r}\sigma_\ell}$ and ν is frequency [Hz].

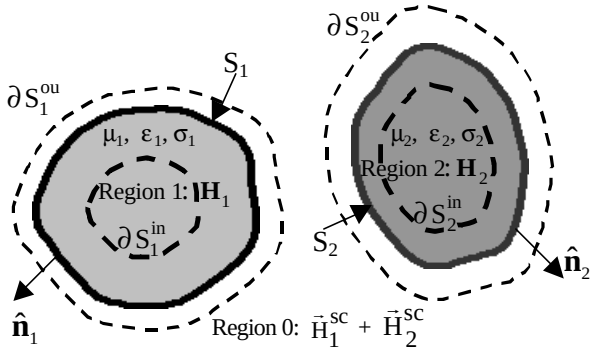

Fig. 2. MAS diagram for multiple objects.

The boundary conditions on the surfaces of the objects specify continuity of tangential components of **H** and normal component of **B**.

On surface S_α:

$$\hat{\mathbf{i}}_{1,a}(\mathbf{r})\cdot\left[\sum_{\ell=1}^{N_{ob}}\mathbf{H}_\ell^{sc}(\mathbf{r})+\mathbf{H}^{pr}(\mathbf{r})\right] - \hat{\mathbf{i}}_{2,a}(\mathbf{r})\cdot\left[\sum_{\ell=1}^{N_{ob}} d_a^\ell\mathbf{H}_\ell(\mathbf{r})\right] = 0. \qquad (2)$$

Here the vectors $\hat{\mathbf{i}}_{i,a}(\mathbf{r})$ consist of two independent tangential and one normal vector at each point on the S_α surfaces, $\alpha = 1,2,...,N_{ob}$. In the case of the tangential vectors, $\hat{\mathbf{i}}_{2,a}(\mathbf{r}) = \hat{\mathbf{i}}_{1,a}(\mathbf{r})$ while for the normal case $\hat{\mathbf{i}}_{2,a}(\mathbf{r}) = m_{a,r}\hat{\mathbf{i}}_{1,a}(\mathbf{r})$

$$d_a^\ell = \begin{cases} 0 \text{ if } \ell \neq a \\ 1 \text{ if } \ell = a. \end{cases} \qquad (3)$$

The hybrid full MAS /MAS-TSA [4], [5] was applied for solving this problem. $\mathbf{H}_\ell^{sc}(\mathbf{r})$ are secondary magnetic fields and they are simulated using auxiliary magnetic charges placed on auxiliary surfaces ∂S_ℓ^{in} [1], [2]. We emphasize that these auxiliary surfaces ∂S_ℓ^{in} are enclosed by the physical surfaces S_ℓ and assume that they radiate in unbounded free space, with region 0 characteristics, giving rise to the secondary field, $\sum_{\ell=1}^{N_{ob}}\mathbf{H}_\ell^{sc}(\mathbf{r})$. Similarly, the $\mathbf{H}_\ell(\mathbf{r})$ is magnetic field produced by auxiliary magnetic dipoles placed on the external auxiliary surface ∂S_ℓ^{ou} and they are assumed to radiate in unbounded homogeneous space filled with ℓ-th target's material properties [1], [2]. Applying boundary conditions (2) at given point produces a linear system of

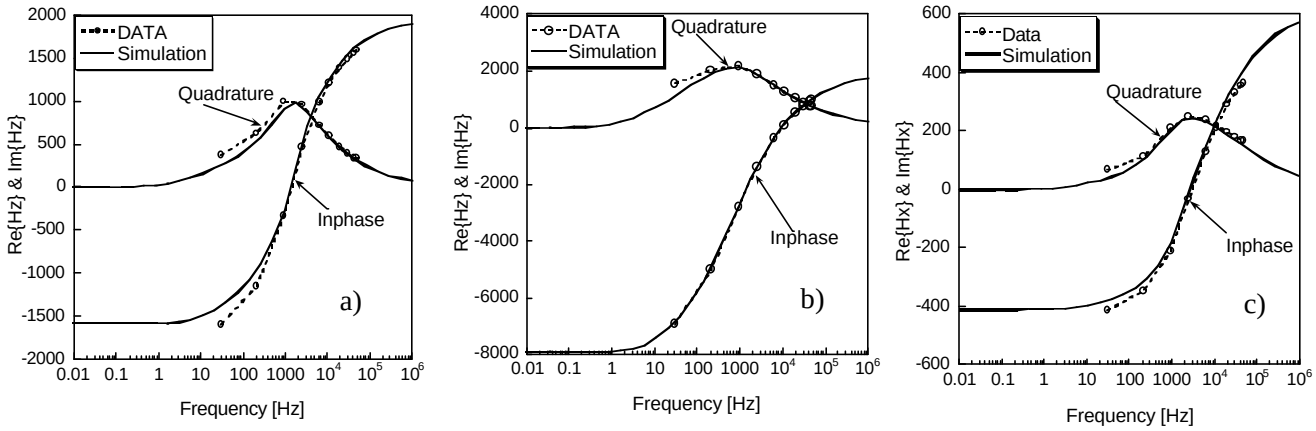

Fig. 3. Scattered magnetic fields versus frequency for two cylinders placed end to end.

equations in which the amplitudes of auxiliary sources are to be determined.

III. Results

To analyze interaction between multiple highly conducting and permeable objects, a computer code was written based on the full MAS and hybrid MAS/MAS-TSA method and several results were extracted and compared to available experimental data.

1. Two cylinders

a. Non-uniform excitation

For the validity of the hybrid full MAS/ MAS-TSA method for multiple targets, we first examine the scattered field for two cylinders illuminated by GEM-3 multi-loop antenna. Cylinders are lined up along the axis of symmetry. The primary magnetic field generated by a GEM-3 sensor was modeled as a field radiated by two concentric coils [2]. The current amplitudes on the coils were chosen such that at the

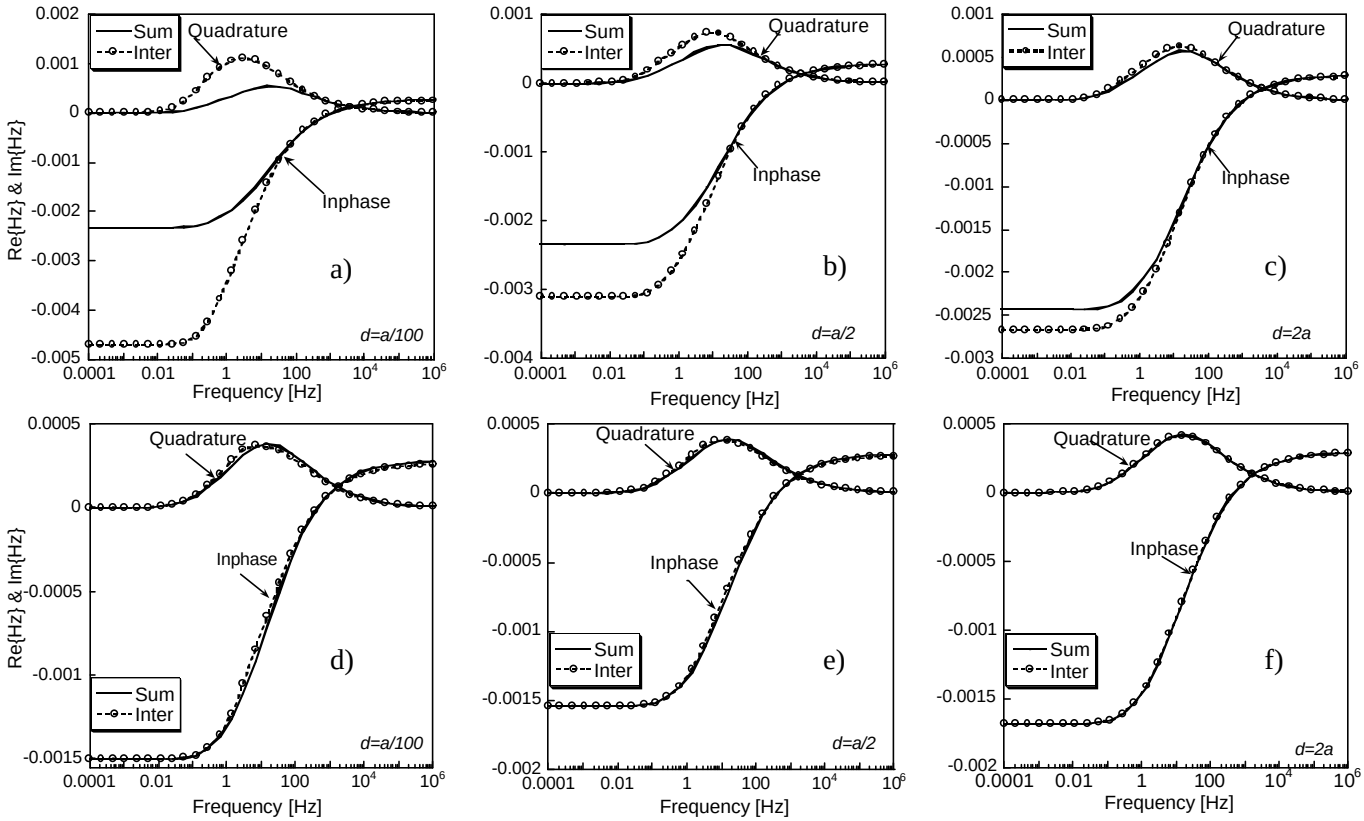

Fig. 4. Secondary magnetic fields versus frequency for two cylinders. Axial excitation: Solid lines correspond to simple summation of responses from each cylinder. Circle lines include interaction between them.

center of the coils the primary magnetic field is zero. Two excitations were considered 1) Axial, i.e. when the coil axes of GEM-3 are aligned with the axis of symmetry of the cylinders and 2) Transverse, i.e. when the GEM-3 axis is orthogonal to the cylinders' axes. In numerical tests for the transverse case, the primary field was considered to be uniform. This assumption is reasonable because the diameter of the cylinders is small relative to the targets' distance from the sensor. The cylinders parameters are: magnetic steel ($L_2 = 3$ inch, $L_2/2a_2 = 2$, $\sigma = 4\ 10^6$ S/m, $\mu_{2r} = 120$) and stainless steel (non-magnetic, L = 3 inch, $L_1/2a_1 = 2$, $\sigma = 1.4\ 10^6$ S/m, $\mu_{1r} = 1$). Fig. 3 a) shows scattered magnetic field versus frequency, when stainless steel is up (i.e. towards the sensor) and the magnetic steel cylinder is down, while the magnetic steel is up stainless steel is down in Fig. 3 b). The observation point is z =31 cm from the middle point between the cylinders. In numerical calculations, the distance between cylinders was assumed to be 10 micrometers. The numerical solution is seen to be in very close agreement with measured data. A similar pattern is observed for transverse excitation in Fig. 3 c).

Note a particular advantage here from using the MAS and MAS-TSA formulations. Conventional integral equation approaches, e.g. MoM, encounter difficulties when two distinct bounding surfaces are very close to one another, as in the example above. Singularities on one surface are close enough to the other surface to disrupt simple integration routines on the latter. They cannot be separated and integrated out analytically in the same way as singularities within a single surface can be. MAS-based methods encounter no such problems, because auxiliary surfaces containing the sources are purposely displaced from the physical surfaces.

b. Uniform excitation

Next we examine broadband EMI scattering from two geometrically identical cylinders (radius a=10 cm, ratio length to the radius is $L/2a$ =3) lined up along the z-axis and excited by a spatially uniform oscillating magnetic field $\mathbf{H}^{pr} = H_o \hat{z}$, $H_o = 1$ (A/m). The cylinders electromagnetic parameters are: for case 1 (Fig. 3 a, b, c) in which both cylinders are the same ($\mu_{1,r} = \mu_{2,r} = 150$, $\sigma_1 = \sigma_2 = 4 \cdot 10^6$ S/m); and case 2 (Fig. 3 d, e, f) in which one cylinder is non-permeable (aluminum, $\mu_{1,r} = 1$, $\sigma_1 = 2.8 \cdot 10^7$ S/m) and one is permeable (steel, $\mu_{2,r} = 150, \sigma_2 = 4 \cdot 10^6$ S/m). Fig. 4 shows comparison of the secondary magnetic fields (inphase and quadrature parts) for the two cylinders with and without interaction included in the calculations. The distances between them are: $a/100$ Fig. 4 a-d:, $a/2$ Fig. 4 b-e: $a/2$ and $2a$. Fig. 4 c-f. Observation point is x=y=0, z=3 m from the middle point between cylinders. These results clearly demonstrate the possibility of significant coupling between metallic objects over entire broadband EMI range. The interaction effects are much larger at low frequencies than at high frequencies. The results also show that the coupling between objects strongly

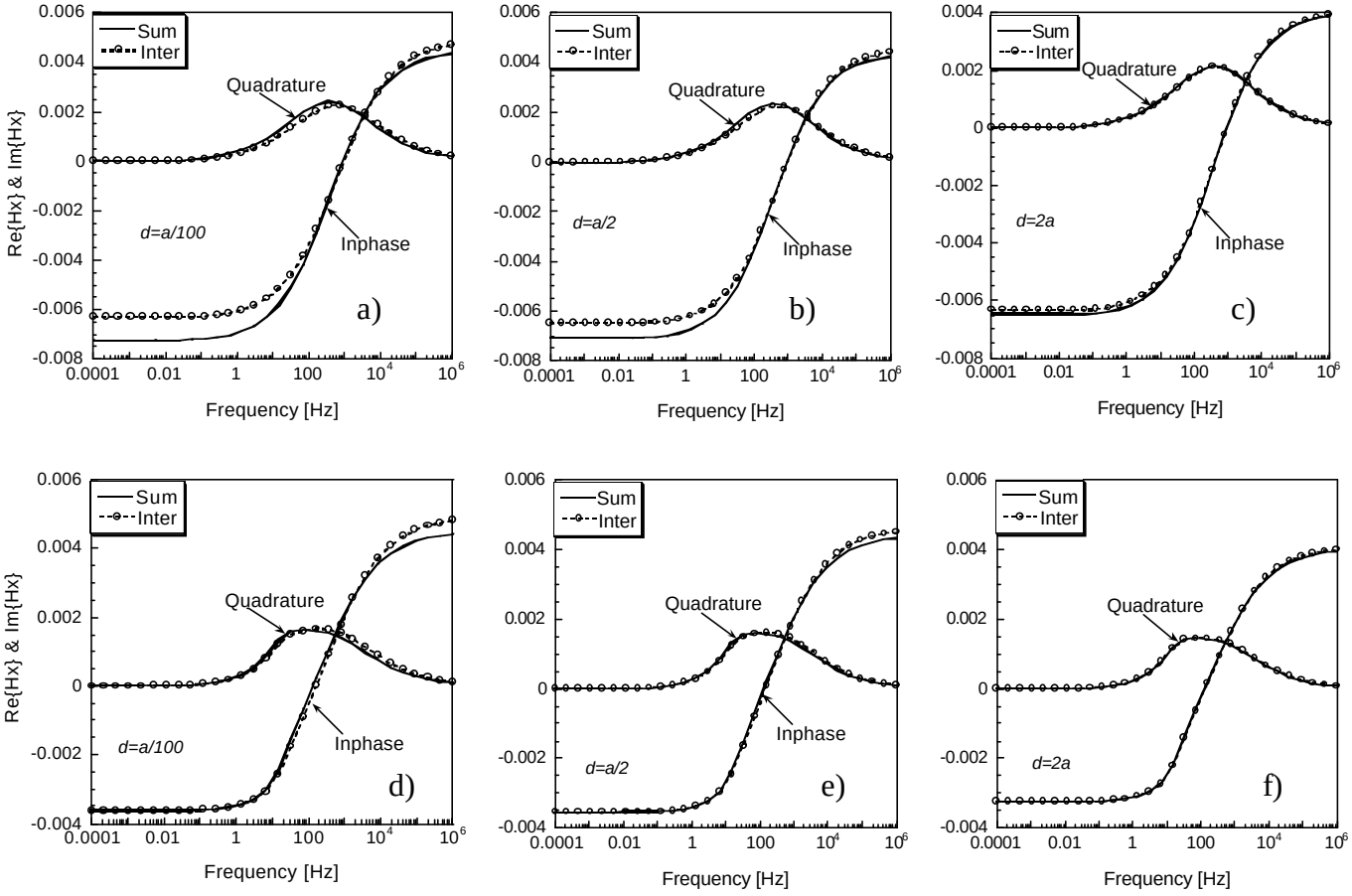

Fig. 5. Secondary magnetic fields versus frequency for two cylinders. Transverse excitation: Solid lines correspond to simple summation of responses from each cylinder. Circle lines include interaction between them.

depends on distances between objects and especially on their material properties. As distance decreases, the difference between the simple summation and full interaction increases greatly, specifically for the two permeable cylinders Fig. 4 a-c. For the two identical permeable cylinders, coupling still exists even when the distance between them is one diameter Fig. 4 c. However, the coupling between non-permeable and permeable cylinders disappears at $a/2$ distance (Fig. 4 e), and is small in any case.

The same cylinders were excited by a time varying uniform magnetic field oriented orthogonal to their axis of symmetry (transverse excitation). Fig. 5 shows the Hx component of the scattered magnetic field versus frequency at the point y = z = 0 and x = 1 m from the middle point between cylinders, for different distances between them: Fig. 5 a, d correspond to separations of a/100; Fig. 5 b) e) for a/2; and Fig. 5 for separation 2a. Again, the results show the existence of coupling between highly conducting and permeable metallic targets in EMI frequency range. At low frequencies the interaction between permeable objects Fig. 5 a-c) is much stronger than between non-permeable and permeable objects Fig. 5 d-f). Additionally, Fig. 5 shows that in case of the transverse excitation the coupling between cylinders is weaker than in axial excitation.

2. Two spheres under uniform primary magnetic field.

Similar tests were performed for two geometrically identical spheres (radius a=25 cm), lined up along the z-axis and excited by a uniform oscillating magnetic field. The spheres' electromagnetic parameters and distances between them are exactly the same as for the cylinders in section III part 1.

Fig. 6 shows EMI responses by the two spheres. In general the effect of interaction between the spheres is similar to that for the cylinders, although the degree of coupling between two permeable cylinders is much greater than between comparable spheres. However, interaction between non-permeable and permeable spheres is stronger than between the comparable cylinders. Overall, at low frequencies the amplitude of EMI responses for interacting permeable targets increases 1.3~2 times (see Fig. 3 a) and Fig. 5 a)). At highest frequencies (PEC) responses decrease, though very slightly.

The same spheres were illuminated by a primary magnetic field oriented transverse to the axis of alignment. The results

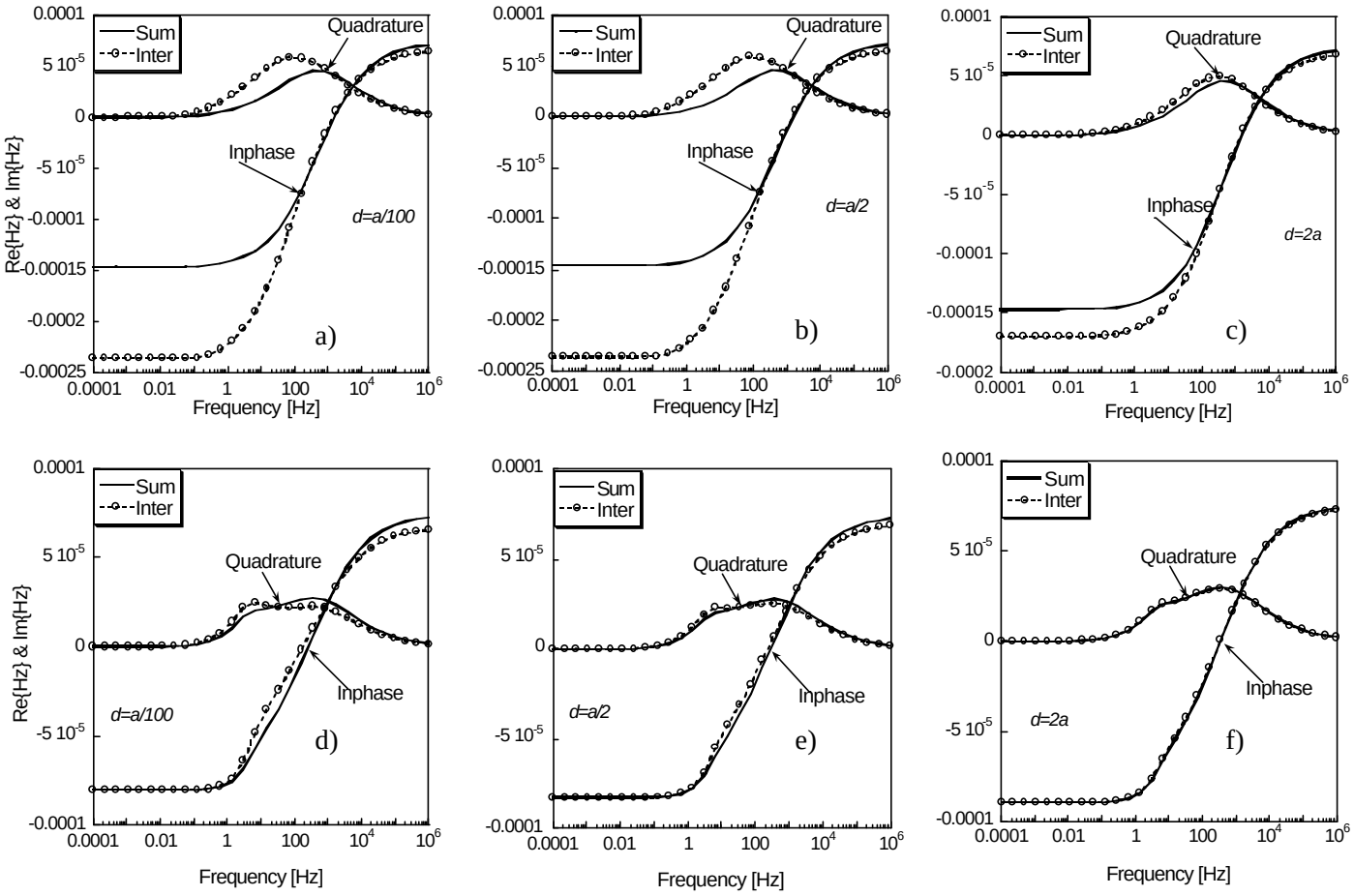

Fig. 6. Secondary magnetic fields versus frequency for two spheres aligned along the Z axis. Axial (Z) excitation: Solid lines = simple summation of responses, circle lines include all interaction between them.

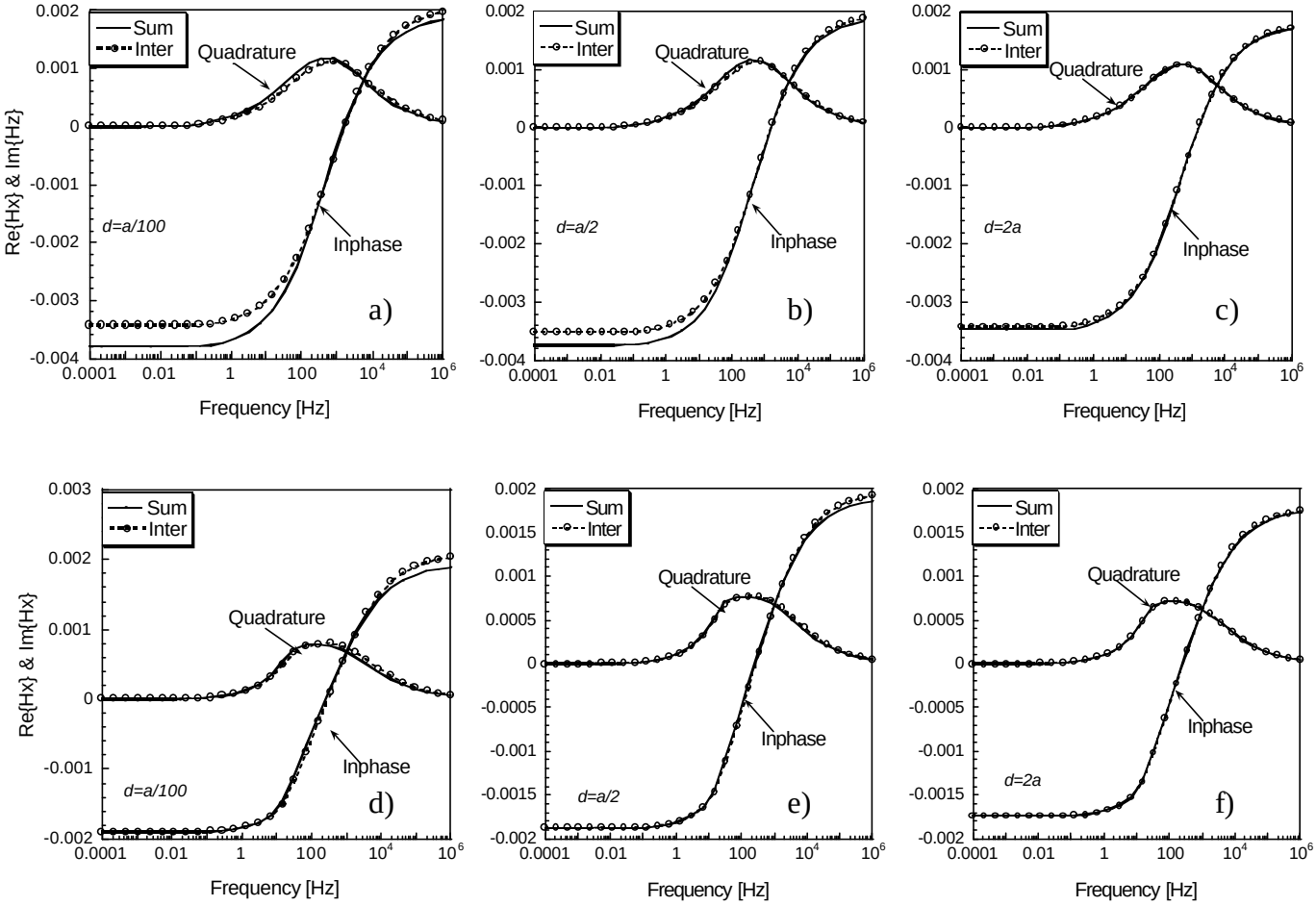

Fig. 7. Secondary magnetic fields vs frequency for two spheres, with excitation transverse to alignment axis: Solid lines = simple summation of responses, circle lines include interaction between them.

are shown on Fig. 7. In general the interaction between spheres for the cases is the same as for cylinders Fig. 5. However, the results show that at high frequencies coupling between cylinders is stronger then between spheres Fig. 5 d) Fig. 7. d).

Near field analysis

In this section we present near field analysis to provide an understanding of the interaction phenomena between metallic objects. Fig. 8 shows equal lines of the total field $\mu_{i,r}|\mathbf{H}_i|$ distributed inside and outside of the two identical objects, where the subscript *i* corresponds to zero for free space and 1or 2 to the first or second targets, respectively. The EM and geometrical parameters are the same as for Fig. 3 b and Fig. 5 b cases, with spheres (a-b) and cylinders (c-d) at different frequencies between 10^{-3} Hz (~magnetostatic limit) and 10^5 Hz (~PEC limit). The distance between objects is 5cm and they are illuminated by uniform primary magnetic field $\mathbf{H}^{pr} = \hat{z}$. Inside permeable metallic object small magnetic dipoles exists. Normally (no external magnetic fields) these dipoles are oriented chaotically and the total field produced by them is zero. When the permeable metallic object is placed inside the low frequency 10^{-3} Hz primary magnetic field, then the primary field forces the internal dipoles to line up in one direction, so that the induced magnetic field is inphase with the primary field and amplifies that field in the external region.

For a single highly permeable sphere under uniform primary magnetic field with unit amplitude 1 (A/m) we see [6] that the amplitude of the total external magnetic field on the boundary approaches a magnitude no greater than about 3 (A/m), no matter how large μ_r is made. Numerical simulations [7] have shown that comparable external fields for the cylinder approach approximately 2~2.5. Fig. 8 shows the amplitude of the total $\mu_{i,r}|\mathbf{H}_i|$ field for permeable spheres (a) and cylinders (c). The field mostly is focused between the objects and increases dramatically from 1 to 4.2 for spheres and from 1 to 8.52 for cylinders. In other simulations we observe that, as two permeable targets approach each other at low frequency, the amplitude of the total field between them significantly increases to factors much greater than those cited above. The stronger magnetic field around each object induces stronger

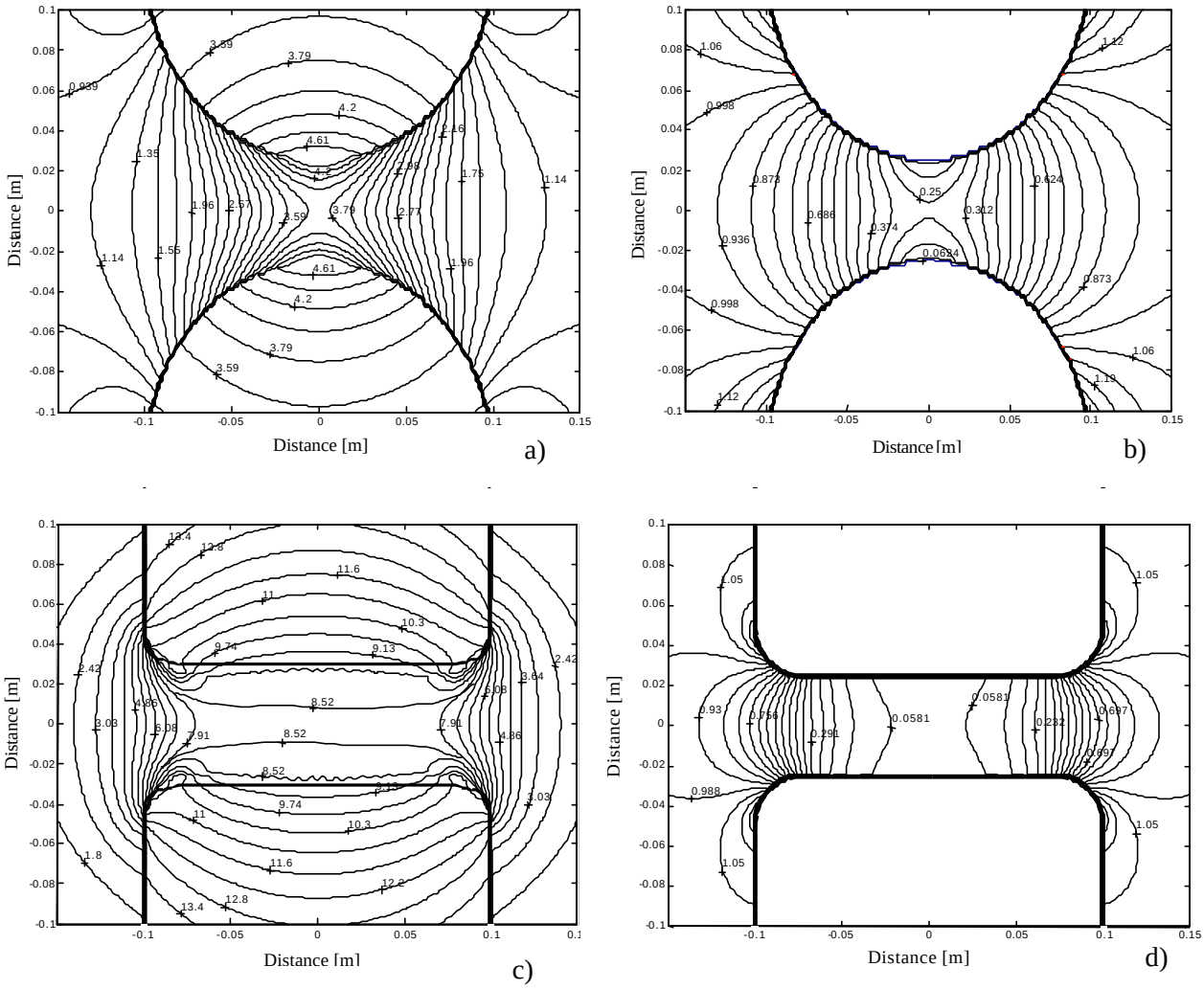

Fig. 8. Absolute value of the total $\mu_{i,r}|\mathbf{H}_i|$ field for axial excitation; left: low frequency; right: high frequency.

response within the other object, which altogether produces stronger far field. By contrast, at high frequencies the induced currents inside object become small, and are distributed only on the surface, opposing the primary magnetic field. When two objects are placed close to each other the total field between objects is suppressed. Figs. 8 b, d show the near magnetic field for the high frequency (~PEC) case. These figures show that the total magnetic fields between objects approaches zero and scattered magnetic fields from the targets are slightly smaller than summation of fields from the separate targets.

In order to understand the underlying physics of transverse excitation (Figs. 5 and 7), Fig. 9 shows contours of the total magnetic field $\mu_{i,r}|\mathbf{H}_i|$ between the same permeable cylinders and spheres as in Fig. 5 and Fig.7. The distance between objects is 5 cm and they are excited by a uniform primary magnetic field $\mathbf{H}^{pr} = \hat{x}$, perpendicular to the line connecting their centers. In these cases the primary magnetic field is parallel to the parts of the spheres and cylinders that are closest to one another. The results show that, at low frequency, the total magnetic fields between the objects are reduced (Fig. 9 a) and c)). This is due to the geometry of the scattered field lines. At low frequency one may think of these lines as radiating from the North pole of each object (on its side in the transverse case), in phase with the primary field, but then arcing around until they are again parallel to but opposed to the primary field in the region alongside the objects. Thus at very low frequency the tangential component of the scattered magnetic field opposes the primary magnetic field between the objects, and total external field is reduced there. According to standard EM boundary conditions, the tangential components of the total magnetic field inside and outside the object must be continuous. Along the line connecting the object centers, the primary and secondary magnetic fields are indeed tangential to the target surfaces. Thus the reduced external field corresponds to a reduced internal field and hence a

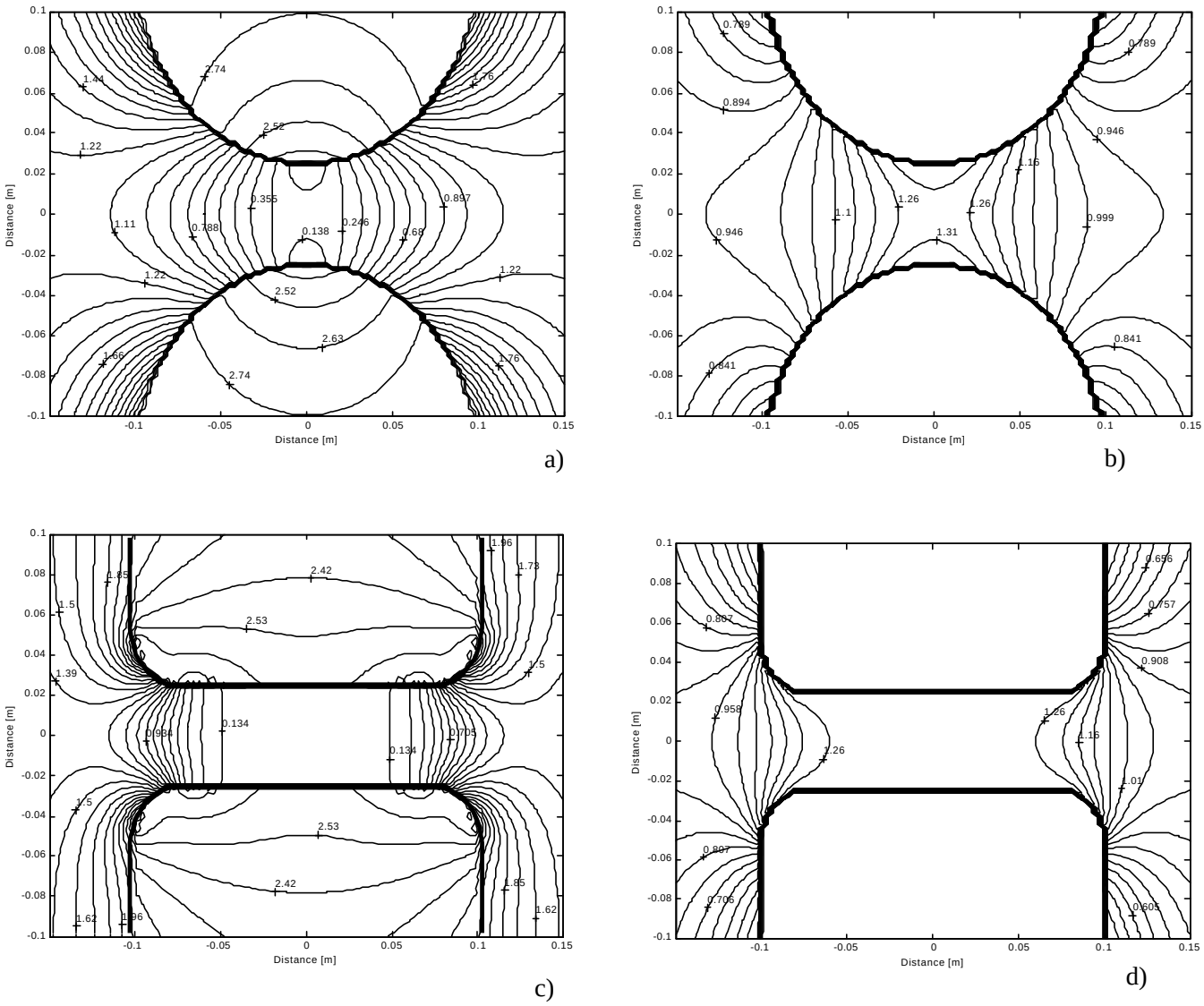

Fig. 9. Absolute value of the total $\mu_{i,r} |\mathbf{H}_i|$ field for transverse excitation; left: low frequency; right: high frequency.

smaller magnetic moment. These facts explain the observation that at low frequency the value of the scattered magnetic field for two objects with coupling Fig. 4 a-c) and Fig. 6 a-c) is smaller than simple summation would predict. At high frequency, the direction of the scattered fields is geometrically similar to those at low frequency, but with sign reversed. Thus the tangential component of the scattered magnetic field between the objects is inphase with the primary magnetic field there. Standard EM boundary conditions near the PEC limit require that the internal fields be negligible, related to the external field by a jump condition, the magnitude of which depends on the induced surface currents. The increased magnitude of the total field between the objects thus corresponds to larger surface currents than would otherwise be present, and hence a larger induced magnetic moment. This is why the results show that the secondary magnetic field from two objects with coupling is slightly larger than predicted by simple summation at high frequency. Because the high frequency phenomenon is associated with induced surface currents, it applies equally to the permeable and non-permeable cases.

IV. Conclusion

In this paper, the hybrid MAS and MAS-TSA is applied for multiple targets, to study electromagnetic interaction problem between highly conducting and permeable metallic objects. The accuracy of the method was tested against experimental data, and numerical tests were performed for combinations of two cylinders and spheres. The numerical method has a distinct advantage relative to popular integral equation

methods because sources of induced EM activity are located on surfaces shifted away from one another.

Overall, significant effects on far field EMI response caused by coupling of multiple objects are observed, depending on the objects' electromagnetic properties, distance between them, their geometries, and orientation of the primary magnetic field. The interaction between aligned permeable metallic cylinders is much stronger than between permeable spheres. Results for target combinations with mixed (non-permeable/ permeable) EM properties show the opposite trend, with the interaction between spheres slightly stronger than between cylinders. However the interaction effects between permeable and non-permeable bodies is slight in any case. Near field analyses have shown that, under axial excitation at low frequencies, the magnetic field is intensified only between permeable targets. Its amplitude increases greatly as the two objects approach each other. Ultimately this increases the magnetic moment of the two-object combination, relative to what would be predicted by simple superposition of responses. This is not the case for permeable/non-permeable combinations at low frequency. By contrast, for transverse excitation the scattered field between permeable objects opposes the primary field at low frequencies and reinforces it at high frequencies. Thus for the transverse case the opposite coupling trend is produced at low frequency, relative to axial excitation. Because high frequency coupling effects in the transverse case are due to induced surface currents, they appear for both permeable and non-permeable combinations. These examinations of near field distributions around the interacting objects show the physical mechanisms responsible for the evidence of coupling seen in the far field, for highly conducting and permeable metallic targets in EMI frequency range.

In future work we explore these effects more comprehensively, organizing them into a suitable basis for inversion or target discrimination.

V. Acknowledgment

This work was sponsored by the Strategic Environmental Research and Development Program and US Army CoE ERDC BT25 and AF25 programs.

References:

1. F. Shubitidze, K. O'Neill, S. A. Haider, K. Sun, and K. D. Paulsen, "Application of the method of auxiliary sources to the wideband electromagnetic induction problem ", IEEE Transactions on Geoscience and Remote Sensing, Vol: 40 Issue: 4, Pages: 928-942, April 2002.
2. F. Shubitidze, K. O'Neill, K. Sun, and K. D. Paulsen, "Investigation of broadband electromagnetic induction scattering by highly conducting, permeable, arbitrarily shaped 3-D objects" IEEE Transactions on Geoscience and Remote Sensing, in press.
3. N. Khadr, B. J. Barrow, T. H. Bell, and H. H. Nelson. "Target shape classification using electromagnetic induction sensor data ". UXO Forum on CD, 8 pages, 1998.
4. F. Shubitidze, K. O'Neill, K. Sun, I. Shamatava, and K. D. Paulsen "A combined MAS-TSA algorithm for broadband electromagnetic induction problems. See in this issue of ACES Proceedings". The 19th Annual Review of Progress in Applied Computational Electromagnetics, Pages: 566-572, March 24-28, 2003.
5. F. Shubitidze, K. O'Neill, I. Shamatava, K. Sun, and K. D. Paulsen "A Hybrid MAS-TSA algorithm for broadband electromagnetic induction problems. See in this issue of ACES Proceedings". Applied Computational Electromagnetics Society Journal, this issue.
6. J. R. Wait, "A conducting sphere in a time varying magnetic field'. Geophysics Volume 16, Pages: 666-672, 1951.
7. I. Shamatava, K. O'Neill, F. Shubitidze, K. Sun, and C. O. Ao. "Evaluation of approximate Analytical Solutions for EMI Scattering from Finite Objects of Different Shapes and Properties", IEEE International Geoscience and Remote Sensing Symposium and 24th Canadian Symposium on Remote Sensing, Pages: 1550 –1552, July 2002.

Fridon Shubitidze received the degree of Diploma radio physicist (M.S) from the Sukhumi branch of Tbilisi State University, Republic of Georgia, in 1994 and Candidate of Sciences Ph.D degree in radio physics (applied electromagnetics) from its physics department, Tbilisi State University, Republic of Georgia, in 1997. Beginning in 1994 he was on the Research Staff of the Laboratory of Applied Electrodynamics, Tbilisi State University, Department of Physics, Republic of Georgia. At the same time he joined department of physics and mathematics, Sukhumi branch of Tbilisi State University as a senior teacher and became Associate Professor there in 1998. From 1998 to 1999 he held a postdoctoral fellowship in National Technical University of Athens, Greece, performing research in connection with computer simulation of electrostatic discharge, electrodynamics aspects of EMC, numerical modeling of conformal antennas, electromagnetic wave scattering, field visualization and identification of objects by scattered field analysis, investigation of wave propagation through anisotropy, plasma and chiral media; and innovative numerical methods. He is currently, working as Senior Research Associate at the Thayer School of Engineering, Dartmouth College, Hanover NH. His current work interests focus on numerical modeling of electromagnetic scattering by subsurface metallic objects.

Kevin O'Neill received the B.A. magna cum laude from Cornell University, followed by M.A., M.S.E., and Ph.D. degrees from Princeton University, Department of Civil Engineering. After an NSF postdoctoral fellowship at the Thayer School of Engineering at Dartmouth College and the U.S. Army Cold Regions Research and Engineering Laboratory (CRREL), he joined CRREL as a Research Civil Engineer. His research has focused on numerical modeling of porous media transport phenomena and of geotechnically relevant electromagnetic problems. He has been a Visiting Fellow in the Department of Agronomy at Cornell University, continues since 1989 as a Visiting Scientist at the Center for Electromagnetic Theory and Applications at MIT, and since 1984 has been on the adjunct faculty of the Thayer School. Current work centers on electromagnetic remote sensing of surfaces, layers, and especially buried objects such as unexploded ordnance.

Irma Shamatava received the degree of Diploma radio physicist (M.S) from Sukhumi branch of Tbilisi State University, Republic of Georgia, in 1994. Since 1997, she has been on the Staff of the Computer center, Sukhumi branch of Tbilisi State University, Republic of Georgia. During the same period she joined Department of Physics and Mathematics, as an assistant teacher. She is currently, working as researcher at the Thayer School of Engineering, Dartmouth College, Hanover NH. Her research interests focus on analytical and numerical modeling of electromagnetic scattering by subsurface metallic objects.

Keli Sun received his B.S., M.S. and Ph.D. degrees in Computational and Biofluid Mechanics from the Department of Mechanics and Engineering Sciences, Peking University, Beijing, P. R. China, in 1991, 1994 and 1997 respectively. As an exchange student, he also worked in the school of Pure and Applied sciences, Tokyo University, Tokyo, Japan, from December 1995 to December 1996, studying the mobility and mechanical properties of membrane proteins in living cells. After getting his Ph.D. degree in 1997, he worked on the faculty of Tsinghua University, Beijing, P.R. China performing research and teaching biomechanics. He obtained a second Master of Science degree in Computational Electromagnetics in May 2001 from the Thayer School of Engineering at Dartmouth College in Hanover, NH. Dr. Sun is currently employed as a Research Associate in the Numerical Methods Laboratory in the Thayer School furthering his research in Computational Electromagnetics and its applications in remote sensing.